How Close Should the Outer Hair Cell *RC* Roll-Off Frequency Be to the Characteristic Frequency?

Mark Ospeck[†*] and Kuni H. Iwasa[‡]
[†]Boulder, Colorado; and [‡]Max Planck Institute for Physics of Complex Systems, Dresden, Germany

ABSTRACT   Recent experiments have shown a much larger conductance in outer hair cells, the central components of the mammalian cochlear amplifier. The report used only the cell's linear capacitance, which together with increased conductance, raised the cell's *RC* corner frequency so that voltage-dependent motility was better able to amplify high-frequency sounds. We construct transfer functions for a simple model of a high characteristic frequency (CF) local cochlear resonance. These show that voltage roll-off does not occur above the *RC* corner. Instead, it is countered by high-pass filtering that is intrinsic to the mammal's electromechanical resonance. Thus, the *RC* corner of a short outer hair cell used for high-frequency amplification does not have to be close to the CF, but depending on the drag, raised only above 0.1 CF. This high-pass filter, built in to the mammalian amplifier, allows for sharp frequency selectivity at very high CF.

INTRODUCTION

The mammalian ear is remarkable in its ability to detect and distinguish faint sound waves at high frequencies: up to ~20 kHz in humans, ~50 kHz in guinea pigs and rats, and >100 kHz for bats, whales, and dolphins (1). This ability depends on prestin, the key component of voltage-dependent somatic motility (electromotility), which is essential for the sensitivity and sharpness of frequency tuning in the mammalian cochlear amplifier (CA (2)). Implied is that voltage-dependent motility amplifies the vibrations of the cochlea's basilar membrane that are elicited by weak sounds. Because motility is driven by outer hair cell (OHC) membrane potential, a key issue is the magnitude of the membrane potential's high-frequency oscillating part. This gives rise to the *RC* time constant problem: OHC have too much resistance (*R*) and capacitance (*C*), the combination of which results in a low-pass filter that attenuates high-frequency voltage oscillations, limiting the characteristic frequency (CF) at which the cells can amplify sound waves (3). Recently, a large-scale cochlear model shows that tonotopic variation of OHC conductance may permit electromotility to function as the CA at high CF (4). Also, models that couple active hair-bundle motion to voltage-dependent somatic motility show improved high-frequency CA performance (5,6). Additionally, piezoelectric resonance has been proposed as a possible mechanism for the CA that avoids the *RC* time constant problem (7). However, a recent series of experiments that were significantly better at preserving the operating conductance of an OHC (8), show that the *RC* roll-off frequency is much closer to the cell's CF than was previously thought. This experimental finding has improved the chances that electromotility will be able to function as the CA at high CF.

The main results reported in this work are the following: OHC hair-bundle conductance and basolateral potassium conductance are much larger than previously reported. The hair-bundle conductance is ~50% open in the resting condition. Therefore, the resting membrane potential is ~−40 mV, much more positive than in previous reports, so that most of the cell's voltage-dependent potassium conductance is turned on at rest. It follows that in quiet, poised at its operating point, the OHC has a very high current throughput. Additionally, and unlike all previous reports, the authors used only the linear component of OHC capacitance (~5 pF for a short one) to calculate the *RC* roll-off frequency. They disregarded the nonlinear capacitance, which near the resting potential of −40 mV is somewhat larger than the linear capacitance for short OHCs. Neglecting nonlinear capacitance increases the *RC* roll-off frequency by a factor somewhat larger than two.

As we will discuss later, their disregarding nonlinear capacitance appears to be justified for the near-isometric case, where the OHC produces force while making only extremely small (<1 part per thousand) changes to its length. Their experiments on cells with a CF of <~12 kHz show a large conductance *g*. For cells in the 1–10 kHz CF range they found that the *RC* roll-off frequency was approximately one-half of the CF. Because their *RC* corner, or roll-off frequency $f_{RC} = g/(2\pi C)$, was now relatively near the CF, they concluded that electromotility is effective as the means of cochlear amplification. Also, by extrapolation, they predict an *RC* corner of ~5 kHz for a gerbil OHC that amplifies sound waves with a 20-kHz CF. However, they note the discrepancy between the CF and the *RC* corner because, for the short OHC used for high-frequency amplification, their *RC* corner rises more slowly than does their CF.

Contrast this with the low-frequency electrically resonant hair cells of the turtle ear whose CF approximately equals

their *RC* corner frequency (9). In the turtle, the electrical resonance where amplification occurs falls a bit below the *RC* corner, and voltage roll-off occurs immediately above it. We note that mammals are distinct from reptiles in that they employ an electromechanical resonance. How close should their *RC* corner frequency be to their CF?

Here we address this question by constructing transfer functions for a simple model of a high CF local resonance. These show that in the mammalian ear, voltage roll-off does not occur above the *RC* corner. Instead, as long as the drag per OHC is not too large, the mammalian amplifier's intrinsic high-pass filtering avoids roll-off. For nominal drag, the electromechanical resonance becomes sharply tuned when the *RC* corner is raised above ~0.1 CF. The new finding of increased outer hair cell conductance (8) has substantially raised the *RC* corner, and intrinsic high-pass filtering combined with the posited range of cochlear drag requires that it only needs to be raised partway to the CF.

RESULTS

When the OHC is isolated, it behaves mainly as a simple passive electrical low-pass filter (its *RC* corner being the frequency at which its voltage begins attenuating with a −1 slope in a log-log plot of voltage versus frequency). However, when incorporated into the organ of Corti, the OHC is not a passive low-pass filter. Instead, the force that it produces acts back upon its hair-bundle conductance so that the cell becomes an active electromechanical resonator that improves the quality *Q*, or sharpness, of its resonance by cancelling local drag force. In 1948, Thomas Gold observed that for a given frequency, if an antidrag were to exactly cancel the drag force, the ear could resonate there and act as a sharply tuned frequency-selective filter (10). Gold's local resonance condition now has the following physical picture: a sound wave at the CF vibrates an OHC hair bundle causing some of the hair bundle's transducer conductance to cycle between its open and closed states, making a sinusoidal current that oscillates the cell's membrane potential at the CF. This voltage oscillation drives voltage-dependent membrane motors that oppose drag force—if their phase is correct. In this way, the drag force can be reduced to near-zero for a resonance oscillation, so that a small input at the CF is amplified.

To obtain insight into how the *RC* time constant affects cochlear amplification and frequency selectivity, we consider its effect upon a high CF local resonance (see the Mathematica (Wolfram Research, Champaign, IL) model in the Supporting Material). The cochlea's basilar membrane actually supports a sound-driven traveling wave that traverses between, and is absorbed by, local resonances. We will discuss how the *RC* time constant might influence the traveling wave later, but here we consider only the *RC* time constant's impact on the transfer function of a simple

two-equation model of a local resonance that involves a single OHC (11). The oscillatory component of OHC receptor potential is described by

$$-C\frac{dv}{dt} = \left(P_0 + \frac{dP}{dx}x\right)g_{HB}(v + V_0 - E_{HB}) + n_0\, g_K(v + V_0 - E_K). \tag{1}$$

We consider only a small membrane potential oscillation (v) at the resting potential (V_0). Equation 1 describes how the potential changes as cell capacitance C is first charged through hair-bundle conductance (g_{HB}), and then discharged through potassium conductance (g_K) at the base of the cell. The hair-bundle conductance open probability $P_0 + (dP/dx)x$ has a static part P_0 ~0.5, its open probability at the cell's resting potential, and an oscillatory part that is a steeply decreasing function of basilar membrane displacement (x). $E_{HB} - V_0$ is the potential drop through hair-bundle conductance to the cell's resting potential, and $V_0 - E_K$ the drop through the cell's basal potassium conductance. By convention, outward current is positive. Note the large standing "silent current" (8,12), with the constant part of hair-bundle input current $P_0\, g_{HB}(V_0 - E_{HB})$ cancelled by the outward potassium current $n_0\, g_K(V_0 - E_K)$. The voltage-gating of the potassium conductance is slow (8) so that its open probability n_0 is a constant that depends on the resting potential.

The equation of motion that governs local movement of the basilar membrane is

$$M\frac{d^2x}{dt^2} = \varphi\, v - D\frac{dx}{dt} - K\, x + F. \tag{2}$$

The electromechanical resonance frequency (CF) is close to the passive mechanical resonance frequency f_0 set by local stiffness (K) and mass (M), where $(2\pi f_0)^2 = K/M$. Basilar membrane acceleration d^2x/dt^2 responds to the total force on the membrane, which is the sum of four terms: motor force, drag force, spring force, and external force. Motor force is due to piezoelectric membrane motor proteins, and for small potential oscillations it can be approximated as a linear function of membrane potential $\varphi\, v$ where φ is the isometric force generated per millivolt (13). The majority of drag force that must be counteracted by a short OHC is thought to be due to shear drag in the gap between the tectorial membrane and the reticular lamina (11,14). Drag due to up-down motion of the basilar membrane can be ignored (15). The drag due to the hair bundle is much smaller than gap drag in the basal turn (11). An upper-bound estimate for internal drag in the organ of Corti is ~60% of the gap drag (11). The gap between the two membranes forms a shear cell with drag force inversely proportional to its width. For low CF, this gap is ~5-μm wide, but at high CF the gap shrinks down ~1 μm (16). Mechanical oscillation of the OHC hair bundle drives the

shear between these two membranes, and this in turn drives the hair bundles of the sensory inner hair cells.

For laminar shear flow between two plates with a relative velocity dx/dt, the drag force is $(\eta A/d)(dx/dt)$, where η is the viscosity, A is the plate area, and d is the width of the gap between them. The value $\eta A/d$ can be calculated to be $\sim 10^{-7}$ Ns/m for a short OHC and this drag coefficient can be considered to be the lower bound for the cell's actual drag coefficient D (see the Supporting Material). External force F is due to the sound wave input. At membrane potentials above -40 mV, approximately one-half of the hair-bundle conductance is activated and most of the cell's potassium conductance is turned on ((8); see Table 1 for parameter values). This model is intrinsically nonlinear in that weak input signals are much more strongly amplified than strong ones (see the Supporting Material). The main source of nonlinearity is due to the hair-bundle conductance, which opens in proportion to basilar membrane displacement according to a sigmoid-shaped first-order Boltzmann open probability (8). Hair-bundle slope conductance $g_s = g_{HB}(dP/dx)$ is the important term in Eq. 1 that must be made sufficiently large to charge cell capacitance on a cycle-by-cycle basis. Slope conductance is a maximum for small sub-1-nm displacements around a 0.50 open probability, and decreases for larger displacements, which has the effect of lowering gain.

Now we use this simple model of a cochlear resonance to illustrate why the mammal's electromechanical resonance is quite distinct from the reptile's electrical one, and specifically why the mammal's resonance frequency (CF) is able to lie well above its *RC* corner. We choose a specific CF to show transfer functions and a pole-zero plot that clarify how this sort of resonance works. Because high-frequency performance is key, we pick a 20-kHz CF to illustrate things, because before these recent experiments (8), OHC conductance was considered too low to allow for amplification and sharp frequency selectivity for such a high CF. Three force-

noise-driven transfer functions are shown for low, high, and max drag (Fig. 1 A). This transfer function gives the amplitude of the basilar membrane response to the same magnitude of forcing at each frequency across a 50-kHz wide range. Whereas the drag force at a cochlear resonance is not experimentally known, the passive Q of a dead cochlea is known to be between 1 and 2 (18). We set it equal to 1.7, reflecting the fact that without active amplification by the OHC a local cochlear resonance rings only weakly and is not very frequency-selective. Then hair bundle and potassium conductance are together increased, maintaining the resting potential while raising the cell's *RC* corner and sharpening the resonance. The major effect of raising OHC conductance is to increase the hair-bundle slope conductance, permitting it to more rapidly charge cell capacitance, thereby increasing the size of the voltage oscillation and membrane motor force. More motor force cancels more drag, increasing the mechanical Q of the resonance. We raise active small-signal Q up to 20, a frequency selectivity that is comparable to some of the best experimental data for a living cochlea (19–21).

If the 20-kHz local resonance were to have a minimal drag coefficient approximately equal to gap shear drag, $D = \eta A/d \sim 10^{-7}$ N s/m, then obtaining a Q of 20 would require only a relatively small hair-bundle conductance ~ 15 nS and a low *RC* corner ~ 0.7 kHz. However, although gap shear drag has been termed essential drag in that it is responsible for driving the sensory inner hair cell's hair bundle (14), and is thought to be a large component of the total drag, it's not likely that the drag force could be so close to its minimum value. Therefore we consider a high-drag example, increasing the drag coefficient by fivefold over this shear drag lower bound. Countering enough of this drag to achieve a $Q = 20$ resonance required a large OHC conductance ~ 77 nS and an *RC* corner ~ 3.7 kHz. Before the recent experiments (8), using such a large hair-bundle conductance and high *RC* corner could not be justified.

TABLE 1 Parameter values in Eqs. 1 and 2 for modeling a cochlear resonance

|	
C	5 pF. Linear capacitance of a short OHC (8).
$\dfrac{dP}{dx}$	$\dfrac{-1}{25 \text{ nm}}$. Maximum slope open probability hair bundle (17).
$E_{HB} - V_0$	120 mV. E_{HB} endolymph potential $+90$ mV$- 0$ mV reversal potential of the hair-bundle conductance minus resting potential -30 mV (8).
$V_0 - E_K$	60 mV. This assumes resting potential -30 mV and a potassium reversal potential $E_K = -90$ mV.
φ	0.1 nN/mV. Isometric force produced by OHC per millivolt (13).
D	$\sim 10^{-7}$ Ns/m $= \dfrac{\eta A}{d}$. Gap shear drag coefficient; minimum drag that must be cancelled to obtain a sharp high Q resonance (11).
g_K	Total potassium conductance, proportional to g_{HB} so that resting potential is fixed at -30 mV with hair-bundle conductance half-open and potassium conductance 0.81 open (8).
f_{RC}	Passive *RC* corner $= g/(2\pi C) = \dfrac{p_0 \, gHB + n_0 \, gK}{2\pi \, C} = \dfrac{0.5 \, gHB + 0.81 \, gK}{2\pi \, C}$ (8).
Passive Q	$= \dfrac{M \, 2\pi f_0}{D} = \dfrac{\sqrt{M}\sqrt{K}}{D} = 1.7$. This depends on local mass M, stiffness K, and drag coefficient D; it indicates the sharpness of a passive mechanical resonance (18).

log bm displacement

A

log voltage

B

Abs[trans fct]

C

D
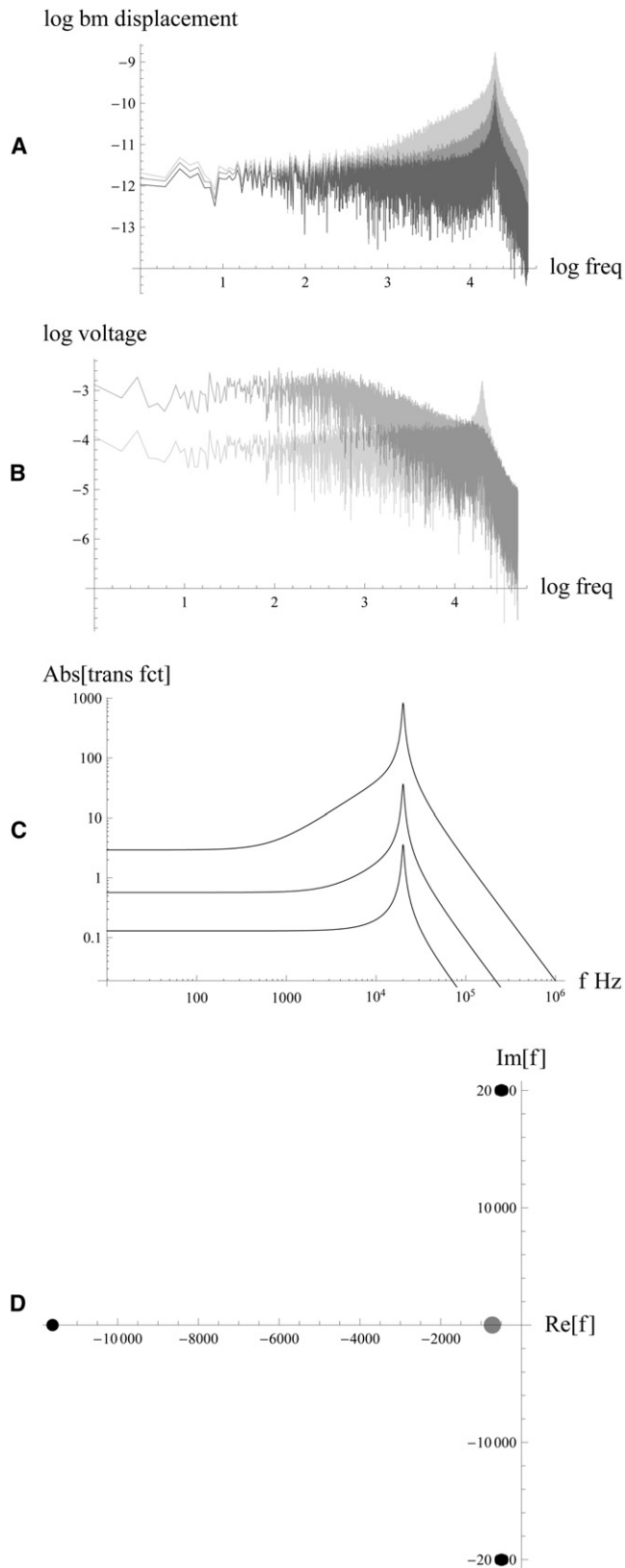
FIGURE 1 (*A*) Noise-driven force to basilar membrane displacement transfer functions for a 20 kHz CF cochlear resonance. (*Top*) Low drag 1.0 10^{-7} Ns/m, hair-bundle conductance 15 nS, *RC* corner 0.7 kHz. (*Middle*) High drag 5.0 10^{-7} Ns/m, hair-bundle conductance 77 nS, *RC*

Finally, we consider roughly the max drag that can be cancelled subject to the constraints imposed by the experimentally measured parameters (Table 1), increasing the drag coefficient by 13 times over its lower bound. To obtain an equally sharp resonance this case required a 12.6 kHz *RC* corner and a very large ~260 nS hair-bundle conductance. Gaussian white-force noise across a 50-kHz bandwidth was used to obtain the spectral shape of the force to basilar membrane displacement transfer functions (22). Although the active *Q* of the resonance peaks are all constrained to 20, their low-frequency spectral shapes differ substantially. In the cases where the *RC* corner is well below the CF, the high-frequency noise gets rolled-up (Fig. 1 *A*). As we will explain below, this is because the oscillatory component of hair-bundle current opposes capacitive current (Fig. 1 *B*). In vivo, the OHC does not behave like a simple low-pass filter whose voltage rolls off above its passive *RC* corner frequency.

We now use the analytic form of the force to displacement transfer functions to show that the hair-bundle current source is acting like an active high-pass filter that opposes voltage roll-off. This form was obtained by assuming small forcing and then linearizing the system (Eqs. 1 and 2; and see details in the Supporting Material). This sort of mechanical force to displacement transfer function is most easily visualized as displacement being inversely proportional to a sum of a pair of differences, the first being the difference between spring force and inertial force. At the resonance frequency (*f* = CF) the spring and inertial forces cancel,

corner 3.7 kHz. (*Bottom*) Max drag 13.0 10^{-7} Ns/m, hair-bundle conductance 263 nS, *RC* corner 12.6 kHz. For each drag case, passive *Q* is set equal to 1.7, then hair bundle and potassium conductance are raised together. This has the effect of increasing motor force that cancels more drag, so that a sharp resonance with an active *Q* of 20 is obtained. The resonance peaks are made to have the same shape, but below CF the frequency responses differ. All three cases are driven by 1.0 pN RMS white-force noise across a 50 kHz bandwidth. (*B*) Current to voltage transfer functions. In the low drag case, when motor force is turned off (*dark*) the voltage rolls-off at the 0.7 kHz *RC* corner, as would be expected for a simple low-pass filter. However, when motor force is turned on (*light*) the voltage does not roll-off at the *RC* corner, because the oscillatory part of hair-bundle current opposes capacitive current. Thermal-sized 0.4-nm RMS hair-bundle noise was used to obtain the spectral shapes. (*C*) By linearizing Eqs. 1 and 2, analytical force to basilar membrane displacement transfer functions were obtained (Eq. 3). Parameters were chosen so that these correspond exactly to the three simulation cases of part A: (*Top*) low drag, (*middle*) high drag, and (*bottom*) max drag. (*D*) Pole-zero plot in the complex frequency plane for the low drag transfer function from part C. Three poles are shown as small solid points and the zero as a larger shaded point located at −0.7 kHz on the negative real axis. This *RC* zero acts to roll-up high-frequency voltage noise, raising part *C*'s transfer function above the corner with a log-log slope ~+1. The hair-bundle current source is behaving like an active high-pass filter, causing voltage roll-up, instead of roll-off. The negative real axis pole at −11.6 kHz is due to the combined effects of capacitance and drag. This arrangement of a pole and zero on the negative real axis is the sign of a high-pass filter. The complex pole pair at (−0.5 ± *i*20.0) kHz is responsible for the *Q* = 20 resonance peak.

leaving only the residual drag force—the difference between drag force and antidrag motor force—to limit the displacement amplitude. It is informative to write this transfer function in its parameter and frequency representations:

specifically, its zeros (complex frequencies where its numerators zeros) and poles (complex frequencies where its denominators zeros). These poles and zeros are then plotted in a pole-zero plot in the complex frequency plane

$$\frac{x}{F} = \frac{1./M}{(2\pi f_0)^2 - (2\pi f)^2 + i\left(2\pi f \dfrac{D}{M} - \dfrac{\dfrac{\varphi g_s}{Mg}(-E_{HB} + V_0)}{i - 2\pi f \dfrac{C}{g}}\right)}$$

$$= \frac{1.}{K - M(2\pi f)^2 + i\left(2\pi f\, D - \dfrac{\varphi \dfrac{g_s}{g}(-E_{HB} + V_0)}{\dfrac{f_{RC}}{f} + \dfrac{f}{f_{RC}}}\right) + \dfrac{\varphi \dfrac{g_s}{g}(-E_{HB} + V_0)}{1. + \left(\dfrac{f}{f_{RC}}\right)^2}}.$$

(3)

Fig. 1 *C* shows analytical transfer functions corresponding to the same low, high, and max drag cases as the simulation transfer functions in Fig. 1 *A*. The frequency representation distinguishes the real part of the membrane motor force that has the correct phase to oppose drag, from its imaginary part that increases the effective spring constant. Note that 2π CF $\cdot$ *D* is the drag force at the CF that must be almost cancelled by motor force to obtain

(Fig. 1 *D*). This sort of plot is well suited for a geometric interpretation of a transfer function. One first chooses a frequency of interest on the positive imaginary axis, draws lines from it to the poles and zeros, and then forms the ratio between the distances to the zeros divided by the distances to the poles. This ratio gives the value of the transfer function for that frequency. In the low drag case, this ratio goes as

$$\frac{(distance\ to\ RC\ zero\ at -0.72)}{(distance\ to\ pole\ at -0.5 - i20)(distance\ to\ pole\ at -0.5 + i20)(distance\ to\ pole\ at -11.6)}.$$

a high Q resonance. Inspection of the frequency representation shows that at CF the phase of motor force is mainly real when the *RC* corner lies well below CF, so that then motor force opposes drag. However, for the max drag case when the *RC* corner is close to the CF, for frequencies near CF the phase of motor force is in between spring force and anti drag. Physically this means that counteracting max drag demands a very large hair-bundle conductance and current that charges cell capacitance quickly so that the resulting fast motor force raises the effective spring constant. In the max drag case, the CF is raised by ~3 kHz above its passive mechanical resonance f_0. The limiting CF where motor force can completely cancel drag force is shown as a function of hair-bundle conductance and drag coefficient in Fig. 2. The figure was obtained by setting drag force equal to the real part of motor force in Eq. 3. High drag and high CF quickly start to require enormous amounts of hair-bundle conductance to achieve sufficient slope conductance to charge the cell on a cycle-by-cycle basis.

There is a third and extremely useful algebraic way to write the Eq. 3 transfer function in terms of its factors:

For example, for *f* near the 20 kHz resonance frequency, the distance in the denominator between *f* at *i* 20.0 kHz and the pole at $(-0.5 + i\ 20.0)$ kHz is very small, hence the large value of the transfer function at resonance. In this way the pole can be seen as being responsible for the resonance peak. The closer the pole to the imaginary axis, the higher the Q and the sharper the resonance. Also, frequencies above the *RC* corner are rolled-up (23) by the action of the *RC* zero because, as *f* increases from 1 to 10 kHz, the distance between *i f* and the zero at -0.72 kHz increases much more quickly than does its distance to the pole at -11.6 kHz. Their ratio increases with rising frequency, increasing the value of the transfer function, hence roll-up. Physically, "roll-up" means that in the frequency range between the *RC* corner and CF, motor force is more than able to counter drag force, amplifying these frequency components. Gold's resonance constraint, requiring that most of the drag force be cancelled at the CF, means that lower-frequency, lower-velocity components see negative drag.

At these frequencies, hair-bundle fluctuations are amplified due to a high-pass amplifier effect that is quite distinct
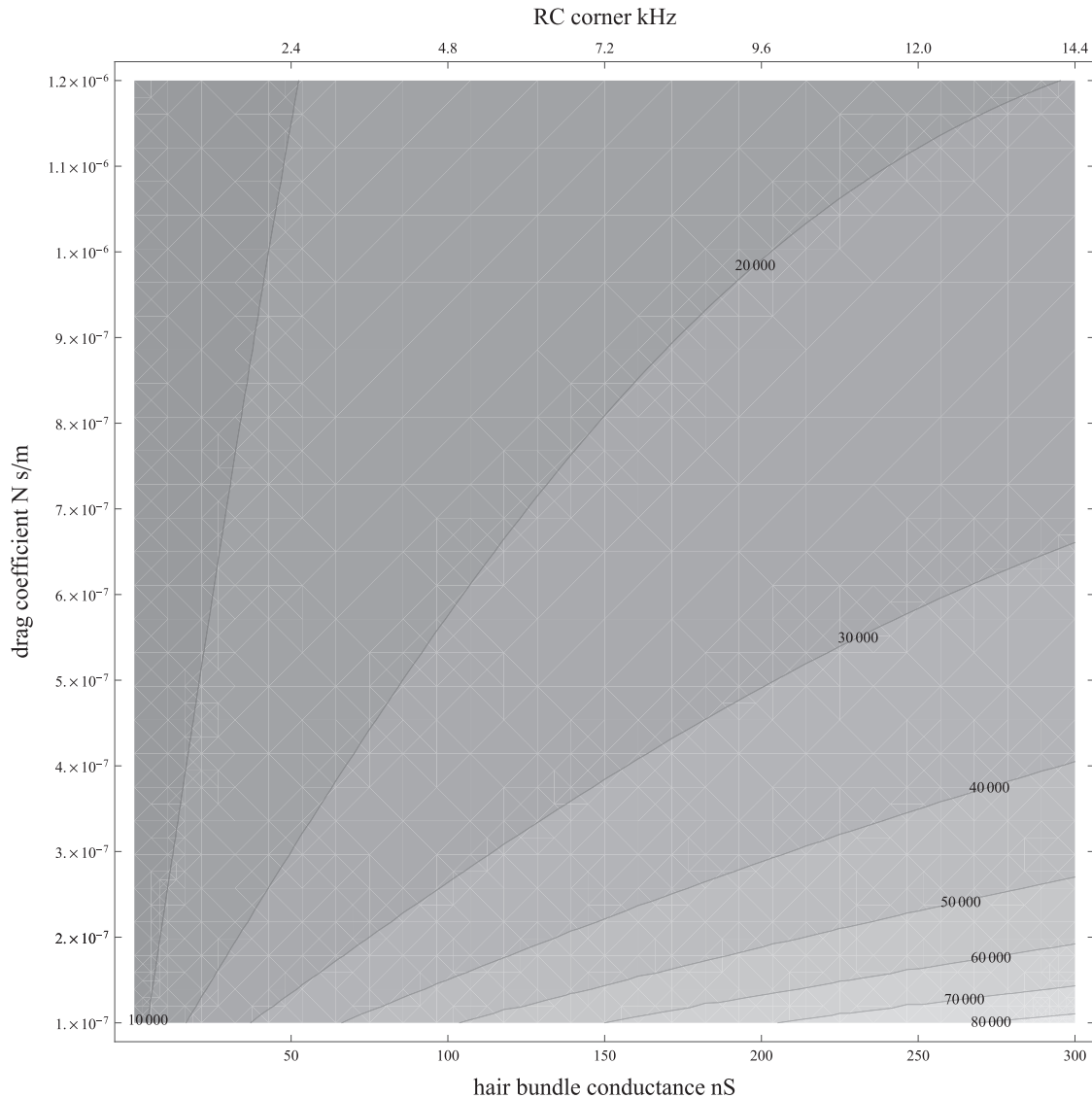
FIGURE 2 Contour plot showing the maximum frequency that is able to support a high Q cochlear resonance, versus hair-bundle conductance and drag coefficient. This result depends on the experimentally measured parameters in Table 1. Slope sensitivity of the hair-bundle conductance dP/dx and isometric motor force per millivolt φ are especially important parameters for high-frequency amplifier performance (see the Supporting Material). Note that setting the hair bundle half-open with the cell's resting potential at -30 mV fixes the RC corner at $1.5\, gHB/(2\pi\, C)$, hence the RC corner is plotted across the top. The plot was obtained by assuming that, at the frequency limit, motor force was able to completely cancel drag force (Eq. 3). Drag force, being proportional to frequency, is limiting. For example, for a high drag coefficient five-times its lower bound ($D = 5.0\ 10^{-7}$ Ns/m), a CF of 30 kHz would require an RC corner frequency close to 10 kHz, and achieving this would require 200 nS of hair-bundle conductance. However, if drag were only twice its lower bound, then a high Q resonance at 30 kHz could be made to work with a 75-nS hair-bundle conductance, and an RC corner at ~3.5 kHz.

from resonance amplification (which is associated with the complex pole pair). This high-pass effect lifts the transfer function below the CF, so that if the drag is not too large, the RC corner can be placed well below the CF. A simple low-pass filter has a single pole on the negative real axis at the RC corner, whereas a simple high-pass filter has a pole on the negative real axis and a zero at the origin. The pole-zero plot shown here has two distinct parts— a complex pole pair that is responsible for the resonance, and a pole-zero pair on the negative real axis that makes an active high-pass filter that lifts the resonance. Physically,

the hair bundle is sourcing a current that opposes capacitive current for frequencies up to the CF. This high-pass filtering preamplifies frequencies in the range below CF, and we speculate below that it would appear to amplify traveling wave components on the basilar membrane that are soon to be absorbed by lower CF resonances. Also, high-pass filtering leads to differences in low-frequency signal rejection between the different drag cases. The $f \sim 0$ noise-floor part of the transfer function is lower with respect to the CF peak for the low drag low RC corner case (Fig. 1 C; ~2.6 log units versus max drag's 1.3 log units).

DISCUSSION

The above analysis shows the consequences of a low *RC* corner, its corresponding *RC* zero, and the resulting high-pass filtering, from the perspective of a local cochlear resonance. The mammalian cochlea responds to sounds by making a traveling wave on its basilar membrane that typically contains many different frequency components (1). Sounds are input at the oval window at the cochlea's high-frequency end, with its high-frequency components being absorbed there by high CF local resonances. The more distal the local resonance, the lower is its CF. The traveling wave shows a steep high-frequency cutoff because at a cochlear location below a particular CF, sound energy at or above that frequency is absent, having already been removed (1). However, at a given high CF resonance, all the lower-frequency components are present within the traveling wave, and frequencies above its *RC* corner are presumably being amplified by high-pass filtering. The issues of high-pass preamplification and low-frequency noise rejection due to the action of the *RC* zero are questions that need to be answered by cochlear mechanics: What is a good CF/*RC* corner ratio that would optimize the traveling wave?

When considering the amplification of small signals at high frequency, is it correct to use only the OHC's linear capacitance? It appears that the cells used for high-frequency amplification are made shorter, in part to decrease their linear capacitance (~5 pF for a short 15-μm-long OHC). However, if outer hair cells are not constrained, then their nonlinear capacitance cannot be ignored, and the cell's total capacitance between -30 and -40 mV is more than twice as large as its linear capacitance (24). It is possible that nonlinear capacitance can be significantly reduced if the motile element in the membrane is prevented from undergoing large conformational changes (25). Such a reduction of nonlinear capacitance could happen if an isometric condition is imposed on the OHC in vivo. In this regard, imposing a virtual isometric condition on OHC is advantageous for electromotility. Not only could the membrane capacitance be significantly reduced, but then the voltage-dependent motor's frequency response would be able to extend out to 80 kHz (26).

In our simulations at high CF, the OHC is constrained by a stiff environment and we are principally concerned with very small, near-threshold basilar membrane displacements that are in the 1-nm range. These would correspond to relative length changes in the OHC that are $\ll 0.1\%$, and would engage $< 1\%$ of the cell's nonlinear capacitance. So for this small displacement range the use of a near isometric force-producing condition for the outer hair cell appears to be justified. Hence, in Eq. 1, we neglect both this small nonlinear capacitance term and also a slightly larger resistive motor current term that is due to piezoelectric reciprocity (27). Together these two terms amount to $< 2\%$ of

the hair-bundle current, and including them would require slightly more hair-bundle conductance to maintain the same quality of resonance.

Our simple treatment of the OHC hair bundle involved relating its transducer conductance open probability to hair-bundle displacement using a first-order Boltzmann function (8). Investigating CA performance near auditory threshold, we considered only basilar membrane displacements in the 1-nm range. Both cochlear partition stiffness and hair-bundle stiffness are increasing functions of CF, and in vivo the OHC hair bundle is firmly imbedded into a stiff tectorial membrane. Hair-bundle transducer conductance is found to be approximately half-open in its resting condition (8). Due to transduction channel gating compliance, when poised half-open, a hair bundle becomes a nonlinear spring that shows a decreasing stiffness with increasing transducer conductance open probability, or vice versa—an intrinsic sort of positive feedback that can make the transducer conductance's half-open point unstable (28). Several CA models now couple active hair-bundle motion to voltage-dependent somatic motility (5,6). Hair-bundle adaptation processes that seek to poise transducer conductance at its half-open point likely would enhance net hair-bundle displacement during OHC elongation and contraction cycles.

In conclusion, recent experiments have shown that outer hair cell conductance is much larger than was previously thought, and this raises the cell's *RC* corner frequency, which in turn raises the frequency limit for cochlear amplification (8). This frequency limit is a decreasing function of drag and an increasing function of hair-bundle conductance. Their experiments show ~60 nS hair-bundle conductance in rat OHC with a CF of 4 kHz that increases to ~75 nS for rat at a CF of 10 kHz. Conductance for higher CF cells has not yet been investigated, but they find that hair-bundle conductance increases approximately threefold from a CF of 0.35 kHz to a CF of 10 kHz. Consider a CF of 50 kHz having OHC with ~130 nS hair-bundle conductance. If the drag were only 1.5 times its lower bound, then a high Q resonance could be obtained with an *RC* corner of only ~6 kHz. We have used a simple model for a high CF local resonance to generate transfer functions that show how their spectral shape is affected by the outer hair cell's *RC* corner frequency. The corner needs to be raised high enough so that the voltage-dependent membrane motors are able to cancel most of the local drag force at the CF. However, if the drag force is reasonably close to its lower bound, then the *RC* corner need not be raised close to the CF. High-pass filtering that is inherent to the mammalian resonance prevents voltage from rolling-off above the *RC* corner. For nominal drag, a sharply tuned high-frequency resonance can be obtained with an *RC* corner above 0.1 CF. Unlike the reptile's electrical resonance, the mammal's electromechanical resonance employs mechanisms that allow it to reach very high frequencies.

SUPPORTING MATERIAL

A Mathematica (Wolfram Research) model and reference (29) are available at http://www.biophysj.org/biophysj/supplemental/S0006-3495(12)00320-7.

Thanks to Dorshka Wylie for editing.

REFERENCES

1. Fay, R. R., editor. 1994. Comparative hearing: mammals. *In* Springer Handbook of Auditory Research. Springer, New York.785–831.

2. Zheng, J., W. Shen, …, P. Dallos. 2000. Prestin is the motor protein of cochlear outer hair cells. *Nature.* 405:149–155.

3. Ashmore, J. 2008. Cochlear outer hair cell motility. *Physiol. Rev.* 88:173–210.

4. Mistrík, P., C. Mullaley, …, J. Ashmore. 2009. Three-dimensional current flow in a large-scale model of the cochlea and the mechanism of amplification of sound. *J. R. Soc. Interface.* 6:279–291.

5. Maoileidigh, D. Ó., and F. Jülicher. 2010. The interplay between active hair bundle motility and electromotility in the cochlea. *J. Acoust. Soc. Am.* 128:1175–1190.

6. Meaud, J., and K. Grosh. 2011. Coupling active hair bundle mechanics, fast adaptation, and somatic motility in a cochlear model. *Biophys. J.* 100:2576–2585.

7. Rabbitt, R. D., H. E. Ayliffe, …, W. E. Brownell. 2005. Evidence of piezoelectric resonance in isolated outer hair cells. *Biophys. J.* 88:2257–2265.

8. Johnson, S. L., M. Beurg, …, R. Fettiplace. 2011. Prestin-driven cochlear amplification is not limited by the outer hair cell membrane time constant. *Neuron.* 70:1143–1154.

9. Crawford, A. C., and R. Fettiplace. 1981. An electrical tuning mechanism in turtle cochlear hair cells. *J. Physiol.* 312:377–412.

10. Gold, T. 1948. Hearing. II. The physical basis of the action of the cochlea. *Proc. Roy. Soc. (Lond.). B. Biol. Sci.* 135:492–498.

11. Ospeck, M., X. Dong, and K. H. Iwasa. 2003. Limiting frequency of the cochlear amplifier based on electromotility of outer hair cells. *Biophys. J.* 84:739–749.

12. Zidanic, M., and W. E. Brownell. 1990. Fine structure of the intracochlear potential field. I. The silent current. *Biophys. J.* 57:1253–1268.

13. Iwasa, K. H., and M. Adachi. 1997. Force generation in the outer hair cell of the cochlea. *Biophys. J.* 73:546–555.

14. Freeman, D. M., and T. F. Weiss. 1988. The role of fluid inertia in mechanical stimulation of hair cells. *Hear. Res.* 35:201–207.

15. Keller, J. B., and J. C. Neu. 1985. Asymptotic analysis of a viscous cochlear model. *J. Acoust. Soc. Am.* 77:2107–2110.

16. Lim, D. J. 1980. Cochlear anatomy related to cochlear micromechanics. A review. *J. Acoust. Soc. Am.* 67:1686–1695.

17. Russell, I. J., G. P. Richardson, and A. R. Cody. 1986. Mechanosensitivity of mammalian auditory hair cells in vitro. *Nature.* 321:517–519.

18. von Bekesy, G. 1960. Experiments in Hearing. McGraw-Hill, NY.

19. Sellick, P. M., R. Patuzzi, and G. K. Yates. 1982. Measurements of basilar membrane motion in the guinea pig using the Mössbauer technique. *J. Acoust. Soc.* 72:131–141.

20. Johnstone, B. M., R. Patuzzi, and G. K. Yates. 1986. Basilar membrane measurements and the traveling wave. *Hear. Res.* 22:147–153.

21. Ruggero, M. A. 1992. Responses to sound of the basilar membrane of the mammalian cochlea. *Curr. Opin. Neurobiol.* 2:449–456.

22. DeFelice, L. J. 1981. Introduction to Membrane Noise. Plenum Press, New York, NY.

23. Senturia, S. D., and B. D. Wedlock. 1975. Electronic Circuits and Applications. John Wiley and Sons, NY.

24. Santos-Sacchi, J., S. Kakehata, …, T. Takasaka. 1998. Density of motility-related charge in the outer hair cell of the guinea pig is inversely related to best frequency. *Neurosci. Lett.* 256:155–158.

25. Adachi, M., M. Sugawara, and K. H. Iwasa. 2000. Effect of turgor pressure on outer hair cell motility. *J. Acoust. Soc. Am.* 108:2299–2306.

26. Frank, G., W. Hemmert, and A. W. Gummer. 1999. Limiting dynamics of high-frequency electromechanical transduction of outer hair cells. *Proc. Natl. Acad. Sci. USA.* 96:4420–4425.

27. Dong, X. X., M. Ospeck, and K. H. Iwasa. 2002. Piezoelectric reciprocal relationship of the membrane motor in the cochlear outer hair cell. *Biophys. J.* 82:1254–1259.

28. Martin, P., A. D. Mehta, and A. J. Hudspeth. 2000. Negative hair-bundle stiffness betrays a mechanism for mechanical amplification by the hair cell. *Proc. Natl. Acad. Sci. USA.* 97:12026–12031.

29. Dahl, D., and D. Kleinfeldt. 1976. Perilymph viscosity as a function of temperature and noise stress. *Ann. Acad. Med. Stetin.* 14:83–86.